Bull Volcanol (1987) 49:467—488

Bulletin of Volcanology

The 1982 eruptions of El Chichon volcano, Mexico (3): Physical properties of pyroclastic surges

H Sigurdsson[1], SN Carey[1], and RV Fisher[2]

[1] Graduate School of Oceanography, University of Rhode Island, Kingston, RI 02881, USA
[2] Department of Geological Sciences, University of California, Santa Barbara, CA 93106, USA

Abstract. Two major pyroclastic surges generated during the 4 April 1982 eruption of El Chichon devastated an area of 153 km^2 with a quasi-radial distribution around the volcano. The hot surge clouds carbonized wood throughout their extent and were too hot to allow accretionary lapilli formation by vapor condensation. Field evidence indicates voidage fraction of 0.99 in the surge cloud with extensive entrainment of air. Thermal calculations indicate that heat content of pyroclasts can heat entrained air and maintain high temperatures in the surge cloud. The dominant bed form of the surge deposits are sand waves shaped in dune forms with vertical form index of 10—20, characterized by stoss-side erosion and lee-side deposition of 1—10 cm reversely graded laminae. A systematic decrease in maximum lithic diameter with distance from source is accompanied by decrease in wavelength and amplitude. Modal analysis indicates fractionation of glass and pumice from the surge cloud relative to crystals, resulting in loss of at least 10%—25% of the cloud mass due to winnowing out of fines during surge emplacement. Greatest fractionation from the -1.0—0.0-Ø grain sizes reflects relatively lower pumice particle density in this range and segregation in the formative stages of the surge cloud. Extensive pumice rounding indicates abrasion during bed-load transport. Flow of pyroclastic debris in the turbulent surge cloud was by combination of bed-load and suspended-load transport. The surges are viewed as expanding pyroclastic gravity flows, which entrain and mix with air during transport. The balance between sedimentation at the base of the surge cloud and expansion due to entrainment of air contributed to low cloud density and internal turbulence, which persisted to the distal edge of the surge zone.

Offprint requests to: H Sigurdsson

Introduction

During the testing of an underwater nuclear device in 1946 at Bikini Atoll in the Pacific Ocean, surface-hugging turbulent clouds composed of gases and water droplets were observed to spread radially from the base of the explosion column at hurricane velocities (Brinkley et al. 1950). These ring-shaped clouds, termed base surges, appeared 10 sec after the initial explosion and were initially thought to be caused by bulk subsidence of the explosion column. The Bikini base surge expanded beyond 4 km from source with initial velocities of 50 m/s, decreasing to 20 m/s at a distance of 1.4 km (Young 1965).

The concept of the base surge was first applied to volcanic eruptions by Richards (1959), who pointed out the similarity in the horizontal spread of the base of one of the Barcena 1952 eruption columns and base surges of nuclear explosions. The same phenomenon was described in 1963 during the phreatomagmatic Surtsey eruption, when *tephra-vapor avalanches* extended several hundred meters out to sea (Thorarinsson et al. 1964). The importance of base surges in the 1965 phreatomagmatic eruption of Taal volcano was demonstrated by Moore et al. (1966) and Moore (1967), who first documented their unique depositional features. Fisher and Waters (1970) and Waters and Fisher (1971) identified the base surge as a density current with deposits that contain characteristic dunelike structures and compared them to antidunes analogous to those pro-

duced during the high flow regime of fluvial systems.

Sparks and Walker (1973) recognized that the concept of surges was not restricted to the base surge of phreatomagmatic eruptions and identified the ground surge as a normal accompaniment of pyroclastic flows. The ground surge deposit, later renamed the pyroclastic surge (Sparks 1976), has been designated as layer 1 of the standard ignimbrite flow unit (Sparks and Walker 1973). Fisher (1979) has described surge deposits which formed concurrently with and lie upon cogenetic pyroclastic flow deposits and proposed the term *ash-cloud* surges be applied to them. Although pyroclastic surge layers occur at the base or top of pyroclastic flow deposits, widespread surge deposits can also occur with only minor and highly localized pyroclastic flow deposits, as is the case for the 1982 deposits of El Chichon volcano and the 79 A.D. eruption of Vesuvius (Sigurdsson et al. 1985).

The discrimination between pyroclastic flow or surge deposits can be difficult and controversial, such as in the case of the blast deposit produced by the 18 May 1980 eruption of Mount St. Helens volcano. This deposit has been variously attributed to emplacement by a pyroclastic surge (Moore and Sisson 1981), as a complex combination of pyroclastic flow and surge (Hoblitt et al. 1981; Hoblitt and Miller 1984; Waitt 1981, 1984) or as a pyroclastic flow (Walker and McBroome 1983). According to Fisher et al. (1986) the deposit was emplaced by a blast surge resulting from transport of an initially fully turbulent sediment gravity flow which developed into a two-part transport system during flowage, i.e., a high concentration bed-load in which movement was nonturbulent and an overriding turbulent surge.

Wohletz and Sheridan (1979) have proposed that surges are initially lean-phase fluidized systems, which deflate due to escape of gases, resulting in transitions from viscous to inertial flow. They concluded that there are three associated bed-form facies, i.e., sand wave, massive, and planar, observed with distance from source in some surge deposits, and these facies reflect the transitions from viscous to inertial flow. Field evidence presented in this paper indicates that this model is inappropriate for El Chichon surges, which form sand-wave bed forms throughout. Fisher and Heiken (1982) and Fisher (1983) suggest that turbulent pyroclastic density currents *(nuees ardentes)*, because of gravity segregation, develop into two parts, i.e., an upper dilute turbulent part and a lower high concentration, nonturbulent bed-load part which separate into concurrently moving viscous and inertial flows. The blast deposits of Mount St. Helens (Fisher et al. 1986) show features that corroborate this idea which causes difficulties with the facies concept of Wohletz and Sheridan (1979). Recently, Fisher et al. (1986) and Fisher and Valentine (1986) suggest that fluidization processes are not applicable to pyroclastic surges during their turbulent mode of movement, an observation independently shown by the field evidence presented herein. The El Chichon surges formed dune structures, that we refer to as sand-wave bed forms, throughout their areal extent and have depositional features indicating a combination of bed-load and suspended-load transport, analogous to the conditions during formation of eolian bed forms. During the 1982 El Chichon eruptions, pyroclastic surges were generated with only minor pyroclastic flow generation. The aim of this paper is to interpret diagnostic features of the El Chichon deposits with regard to mode of transport of the surges and their relation to pyroclastic flows.

The 1982 eruptions

From 29 March to 4 April 1982 three large explosive eruptions occurred at El Chichon volcano in southern Mexico (Sigurdsson et al. 1984). These events have become widely known for the unprecedented quantity of sulfuric acid aerosol which formed in the Earth's stratosphere as a result of the eruptions. Another exceptional feature of this volcanic activity was the generation of devastating pyroclastic surges, which destroyed nine villages and claimed the lives of up to 2000 people. The eruptions and the stratigraphy of the pyroclastic deposits have been described elsewhere (Sigurdsson et al. 1984) and quantitative models of the evolution of the Plinian eruption columns and tephra fallout have been presented by Carey and Sigurdsson (1986).

The first eruption which began at 0532 UT on 29 March (eruption A-1) was a ca. 6 h Plinian event. It blasted a new vent in the prehistoric summit dome of the volcano and formed an eruption column with average height of 20 km. It deposited a 0.10 km^3 (DRE, dense rock equivalent) mappable tephra-fall layer (A-1) to the east of El Chichon, but extrapolation of deposit thickness to 1 μm gives a total erupted volume of 0.60 km^3 (DRE), indicating an average mass eruption rate of 3.5×10^7 kg/s. In comparison, the average mass eruption rate during the Plinian phase of the 18

May 1980 Mount St. Helens eruption was 1.94×10^7 kg/s (Carey and Sigurdsson 1985).

After five days of minor phreatic and phreatomagmatic explosive activity, the second major eruption began at 0135 UT on 4 April and lasted for ca. 4.5 h (eruption B). This complex event began with an explosion which produced a low, incandescent eruption cloud around the summit of the volcano, as witnessed by Dr. L. Silva and others from Ostuacan, 11 km to the west. From this cloud issued the first pyroclastic surge (S-1) which devastated the flanks of the volcano (Fig. 1) and spread in all directions, but mainly to the south, up to 8 km from the crater. Minor pyroclastic flows and debris flows from the disintegrating dome also accompanied the first stage. Immediately following the surge a Plinian eruption column developed, from which fallout layer B was deposited. From the distribution of lithics in the fall deposit, it is clear that this eruption column was the most energetic of the El Chichon eruptions (Sigurdsson et al. 1984), with an average column height of 24 km (Carey and Sigurdsson 1986). The B Plinian event also had the highest mass eruption rate, at 6×10^7 kg/s, producing a total of 0.39 km^3 (DRE). Significantly, tephra from this eruption shows the lowest degree of fragmentation, which may in part account for the different behavior of the eruption column. The Plinian stage was followed by a second pyroclastic surge (S-2), which spread radially from the crater and covered 104 km^2. Because of this sequence of events from a Plinian column to a surge, we propose that the second surge originated during column collapse. It was accompanied by minor pyroclastic flows.

The final eruption began at 1122 UT on 4 April (eruption C) and had a duration of 7 h. The Plinian eruption column had an average height of 22 km and produced 0.40 km^3 tephra (DRE) with an average mass eruption rate of 4×10^7 kg/s. This eruption also terminated with a small surge (S-3) with an area of 39 km^2, which is also attributed to column collapse. Total production during the 1982 eruptions was thus 1.09 km^3 (DRE), consisting dominantly (85%) of trachyandesite tephra fall with a relatively minor proportion of surges (12%).

Field relationships

In our field studies of the 1982 El Chichon pyroclastic surge deposits during June 1982 and January 1983 we obtained good coverage in all areas except the northwest sector of the volcano. At this time the young deposits were very well exposed and already deeply incised by erosion, but free of vegetation. The surge deposits blanket all the terrain with a tendency to thicken in depressions and valleys and are thin or absent on the steepest ridges. Because of the presence of three distinctive pumice-fall layers from the 1982 Plinian phases (eruptions A-1, B, and C), determination of the stratigraphic relationships of the surge deposits was straightforward. The distribution of the

Fig. 1. Typical destruction by surges of cinder block and concrete structure in the village of San Isidoro Tanchichal, 4 km southwest of the crater. Deposit is 1 m thick. Note field of sand waves in background

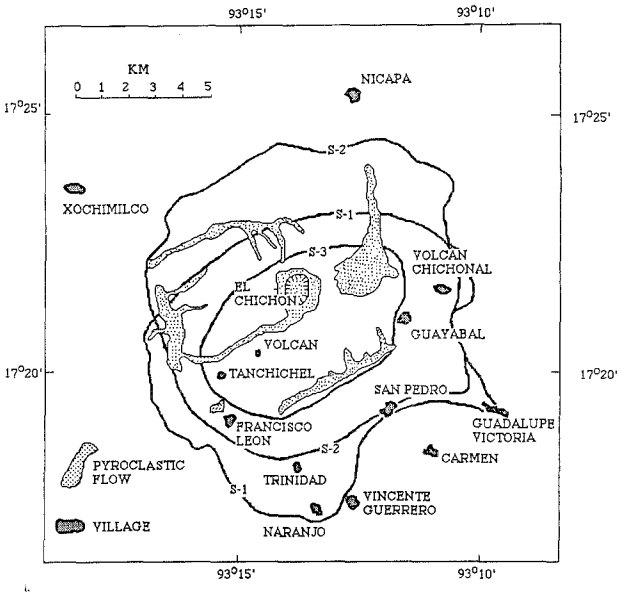

Fig. 2. Areal distribution of the three surge deposits and pyroclastic flows from the 1982 eruptions

three surge deposits and associated pyroclastic flow deposits is shown in Fig. 2. The stratigraphic features of the surges at various locations around the volcano are summarized in Figs. 10, 12, and 13 in Sigurdsson et al. (1984). In this paper, the field relationships and physical properties of the two major surges (S-1 and S-2) are presented. The small third surge (S-3) formed the topmost deposit from the 1982 eruption. It was rapidly eroded by tropical rains and therefore remains unstudied.

The surge deposits were studied in greatest detail in 20 outcrops along a section east of the volcano extending 3.6—6.4 km from the crater. Along this section and in most of the region the first surge (S-1) usually rests directly on the A-1 Plinian pumice fall deposit. Beyond 4.4 km from the crater, however, the 3—5-cm silty A-2 phreatomagmatic fall deposit from the minor eruption at 0840 UT on 3 April is preserved between the A-1 fall and the first surge (S-1). These relations indicate that about 3 km from the crater, the first surge removed the A-2 ash layer and 2—4 cm of the A-1 pumice fall and sandblasted tree stumps protruding out of the surge deposit. It was not erosive beyond 4.4 km. Within 3 km from the crater S-1 was highly erosive on ridges and scarps, where it generally removed the A-1 fall deposit, topsoil, and in some cases eroded into Tertiary sedimentary bed rock, resulting in local concentrations of sandstone and siltstone clasts in the surge deposit.

The first surge deposit (S-1) is invariably poorly sorted and consists of at least two units of equal thickness, i.e., a lower reddish-gray unit and an upper gray unit. No fall deposit or fine-ash layer separates these units. Both units are pumice rich, but lithic fragments are more abundant in the lower unit, giving it the reddish color. The dominant bed form in the S-1 surge are sand waves, consisting of abundant 1—10-cm laminae (Fig. 3). Sand waves are less developed in the

Fig. 3. Cross section of the leeward portion of a dune composed of deposits from the S-1 and S-2 surges. Note the subparallel laminae. Scale is 2 m

lower reddish unit, which tends to become massive in some outcrops. Charcoal from carbonized vegetation is abundant in the lower unit. Stumps of trees and shrubs protruding up into the surge are similarly carbonized or charred and bent in the downrange direction close to the ground. The S-1 surge contains some coarse pumice-rich lenses, which are most common on dune crests or on the lee side of dunes.

The second surge deposit (S-2) generally overlies the pumice fall deposit from the Plinian phase of eruption B. There is some indication of up to 50% erosion of the pumice fall by the surge over a wide area and locally the fall layer has been completely removed. The S-2 surge is generally more pumice rich and lighter in color than S-1 and fine laminae and wave forms are better developed (Fig. 4). The laminae are 1—10 cm in thickness and commonly reversely graded with a pumice-rich top. The dip of laminae is generally 10°—20°. Individual laminae are generally truncated on the stoss-side of dunes, but can be traced for several meters on the lee side. The base of the surge tends to be finer grained and more massive than the central part, which is pumice rich and coarser grained. The topmost part is very well laminated and finer grained. The S-2 surge as a whole is thus reversely graded in the lower half and normally graded to the top. This grading is accompanied by a systematic migration of dune crests at any given locality. In the lower half of the surge deposit, crests of sand-wave dunes migrate downrange, whereas they migrate uprange in the upper half. Lenses of well-rounded pumice are abundant in this surge and usually occur on the lee side of dune crests.

Within 3.5 km east of the crater prominent massive and poorly sorted pumice-rich lenses, ranging 10—60 cm in thickness, appear in the middle of the S-2 surge (Fig. 5). In valleys east, south, and north of the volcano, these lenses are in the distal part of a pumice-rich pyroclastic flow. In proximal areas, the S-2 surge is therefore split into a 0.5—1-m-thick cross-bedded ground-surge layer at the base of the pyroclastic flow and an upper surge with sand-wave beds on top of the flow (Fig. 6). Where it occurs in association with the pyroclastic flow, the two components of the S-2 surge are lithologically identical to the more distal parts of the surge deposit where the pyroclastic flow is absent, except that the surge is generally coarser grained in the more proximal sections bearing the pyroclastic flow. Thus, the pyroclastic flow deposit which occurs in the center of the S-2 surge in proximal sections, is replaced in distal sections by a coarse, pumice-rich component of the surge, merging into the ash cloud and ground-surge components above and below.

Area and mass

The S-1 surge extended asymmetrically over an area of 93 km^2, largely to the south of the volcano (Fig. 7a). S-2 had a more radial distribution and affected 104 km^2 of land (Fig. 7a). The minor

Fig. 4. Detail of internal structures in the S-2 surge deposit, 4.5 km east of the crater. Note the concentration of large rounded pumices and reverse size grading in some of the laminae. Scale is 70 cm

Fig. 5. Massive, poorly sorted lens with large, angular pumice clasts in center of S-2 surge. The lens grades upslope into a pyroclastic flow deposit (see Fig. 6), while downstream it correlates with the well-stratified sandwave deposits of S-2. Scale is 120 cm

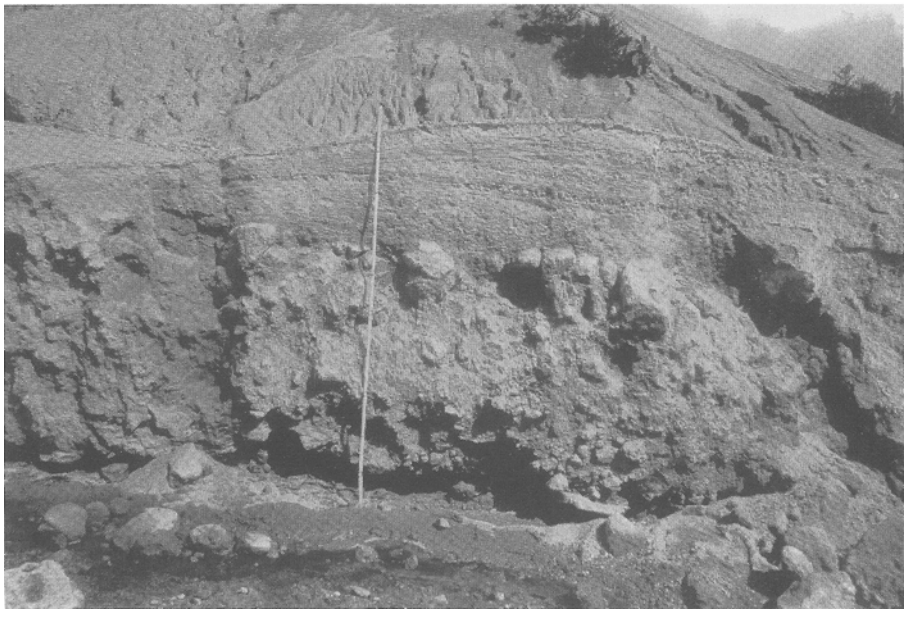

Fig. 6. Pyroclastic flow unit interbedded with the S-2 surge deposit 3.5 km east of the crater with a cross-bedded upper part of the S-2 surge on top, analogous to an ash-cloud surge bed. Scale is 2 m in length

third surge (S-3) extended over 39 km^2. The total area affected by surges and pyroclastic flows around El Chichon is 154 km^2. In comparison, the 1980 Mount St. Helens blast extended over an area of 527 km^2 (Moore and Sisson 1981).

Although of different magnitude and origin, the El Chichon surges from column collapse and the Mount St. Helens blast surge from a directed blast left deposits with very similar thickness/area characteristics. These surge deposits accumulated within a relatively restricted area (Fig. 8), compared to associated fall deposits. The Mount St. Helens blast deposit and the El Chichon surges also exhibit similar isopach/volume relationships (Fig. 9), with a large proportion of the volume within the high isopach range, unlike the associated fall deposits. The volume of the S-1 and S-2 surges is 6.5×10^7 m^3 and 9×10^7 m^3, respectively,

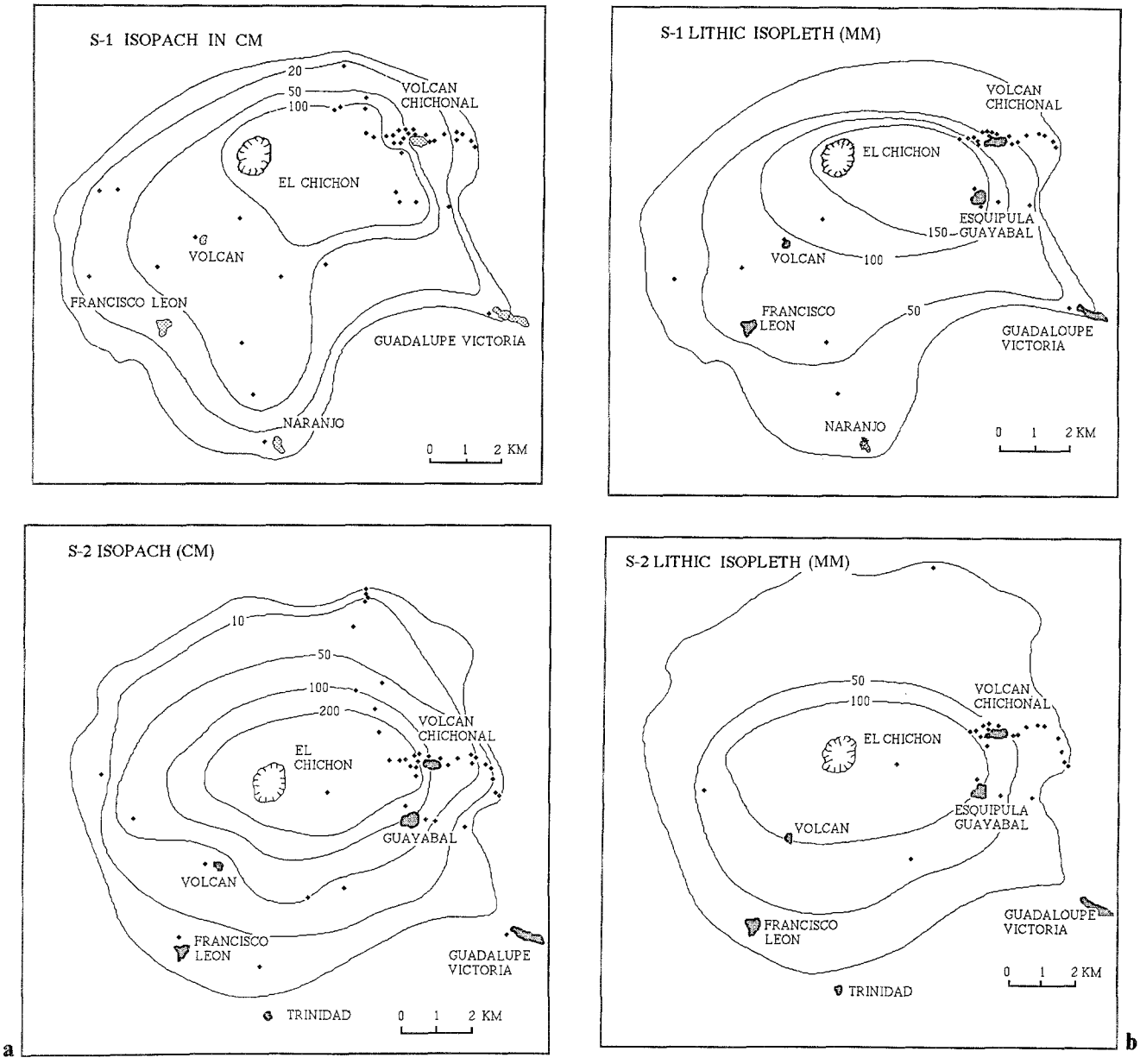

Fig. 7. a Isopach maps of the S-1 and S-2 surge deposits. **b** Maximum lithic isopleth maps of the S-1 and S-2 surge deposits

and their total volume of 0.16 km^3 is identical to the volume of the Mount St. Helens blast deposit (Moore and Sisson 1981).

The lithic isopleth maps of the El Chichon surges are shown in Fig. 7b. They are based on measurements of maximum diameters of the ten largest lithic clasts at each locality. The relationship between maximum lithic sizes and the area enclosed by the lithic isopleths has been used as a basis for comparison of pyroclastic flow deposits and the 1980 blast deposit from Mount St. Helens by Walker and McBroome (1983). They maintain that the latter shows similarity with the lithics/area distribution of typical pyroclastic flows and proposed, partly on these grounds, that the Mount St. Helens blast was a pyroclastic flow. In Fig. 10 the El Chichon surges are compared on a lithics/area plot with several pyroclastic flows and the Mount St. Helens blast deposit. Also shown is the 1982 layer-B fall deposit from El Chichon. This plot shows that the surges and the blast deposit have similar lithic distribution characteristics, and that they differ in general from pyroclastic flows. The diagnostic value of such a

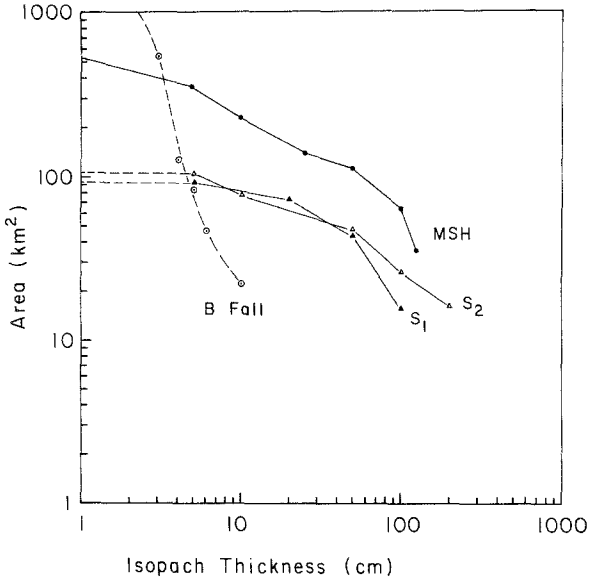

Fig. 8. Relationship between the area enclosed by and the thickness value of isopachs for the S-1 and S-2 El Chichon surge deposits, and the 18 May 1980 Mount St. Helens (MSH) blast (Moore and Sisson 1981). The surge and blast deposits show very similar distribution with most of the mass in the proximal region, in contrast to the distal spread of the El Chichon 1982 B pumice fall deposit

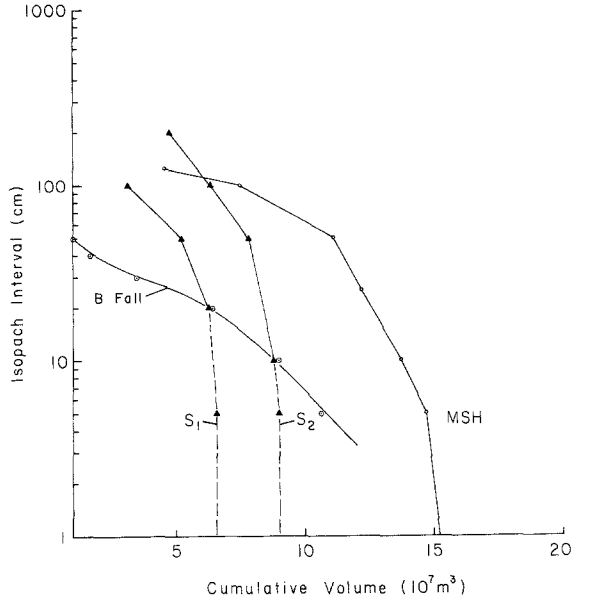

Fig. 9. A plot of isopach versus cumulative volume for El Chichon surges S-1 and S-2 and the 18 May 1980 Mount St. Helens blast deposit (Moore and Sisson 1981). Included for comparison is the B pumice fall deposit from El Chichon

plot in distinguishing surges from flows is not clear, however, and we note for example that the trend of the B fall deposit parallels that of pyroclastic flows.

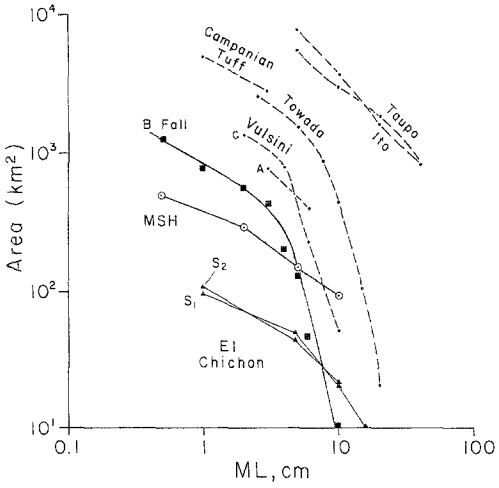

Fig. 10. Plot of area enclosed by isopleths of maximum lithic size (ML) for El Chichon surges S-1 and S-2 and Mount St. Helens blast deposit (Moore and Sisson 1981). Included for comparison are the pumice fall deposit from the B eruption of El Chichon and data from Towada, Taupo, Ito, and Campanian pyroclastic flow deposits (Walker and McBroome 1983)

Wavelength and amplitude

The El Chichon surge deposits are characterized by dune structures, which we call sand waves, throughout their area of deposition. These features are best developed and preserved in relatively flat areas, such as the sites of the villages of Vulcan to the east (Fig. 11) and San Isidoro Tanchichal to the southwest of the volcano. In these areas, the sand waves form transverse, sinuous ridges up to 100 m in length with horizontal form index (breadth/wavelength) ranging 1—10. They are generally asymmetrical with steep stoss and gently sloping lee sides, but more symmetrical forms are also common. Stoss sides are commonly concave upward and almost invariably eroded. Dune crests are generally flat with a gradual increase in slope to about 20° on the lee side. Many dunes are composite, built up by two or three successive sand waves separated by cross-cutting unconformities related to major stoss-side erosion. Lee-side erosion is less common on the other hand, and the lee is characterized by subparallel, 1—10-cm-thick laminae.

In the proximal area the dimensions of dunes are difficult to establish owing to their great wavelength, a relationship also noted by Fisher and Waters (1970) at Zuni Salt Lake crater, New Mexico. At distances greater than 4 km from El Chichon crater, however, dune dimensions are easily measured and there is a systematic relationship

Fig. 11. a Aerial view of the sand-wave field which buried Vulcan village, about 4.5 km east of the crater. Surge-cloud flow direction from right to left. Note larger elongate transverse bed forms up to 100 m in length and smaller transverse bed forms with short and curved crests. **b** Sand-wave field over Vulcan village

between both dune amplitude and wavelength as a function of distance (Fig. 12). Here, wavelength ranges from about 40 m to 1 m and amplitude 4—0.2 m. Systematic decrease in dune wavelength in pyroclastic surge deposits has been noted at Taal volcano (Moore 1967; Waters and Fisher 1971) where wavelengths up to 19 m were attained during the 1965 eruption. The wavelength relationships in four other base surge deposits have also been documented by Wohletz and Sheridan (1979). The wavelength of El Chichon surge dunes is compared with measurements of several other surge deposits in Fig. 13. In all cases there is a decrease in wavelength with distance, but the El Chichon dunes have a higher wavelength and occur at greater distance from source than all other documented dune-bedded surge deposits. On the flanks of the volcano 1—3 km from the crater the surge deposits are discontinuous, gently undulating, and flat-lying with the appearance of planar beds. However, if the dune wavelengths at greater distances are extrapolated toward the source to

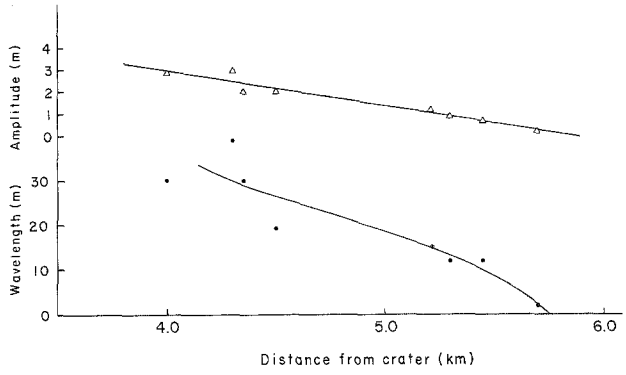

Fig. 12. Relationship between wavelength and amplitude of El Chichon sand waves as a function of distance from source

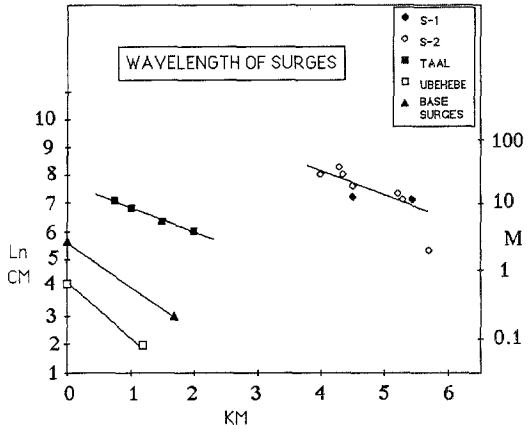

Fig. 13. Variation in sand-wave wavelength (natural log in cm) with distance from source for El Chichon (S-1 and S-2), Taal (Waters and Fisher 1971), and Ubehebe (Crowe and Fisher 1973). The *line* connecting *closed triangles* is best fit linear regression to data from three base surge deposits (Wohletz and Sheridan 1979)

Table 1. Grain-size characteristics of surges

Sample	Ø 5	Ø 16	Ø 50	Ø 84	Ø 95	s Ø	Md Ø	F1	F2	a Ø
S-1:										
EC-207	−2.5	−1.4	0.5	2.2	3.10	1.8	0.5	62.1	1.2	−0.04
EC-193	−2.4	−0.7	1.5	4.3	—	2.5	1.5	77.4	18.0	0.11
EC-206	−0.7	0.1	1.2	2.7	3.90	1.3	1.2	85.1	4.8	0.17
S-2:										
EC-160	−1.3	0.1	1.6	3.1	4.70	2.2	1.6	86.0	9.2	0.01
EC-69	−1.5	−0.1	1.4	2.9	4.10	2.2	1.4	83.5	5.3	0.02
EC-70	−3.4	−0.9	1.0	2.4	3.70	2.9	1.0	74.7	3.6	−0.09
EC-102	−2.4	−1.2	0.4	1.9	2.80	2.1	0.4	61.7	2.1	−0.04
EC-62	−3.9	−1.5	2.0	4.4	6.70	2.9	2.0	77.2	19.8	−0.16
EC-63	−0.6	0.6	1.8	3.5	6.00	2.0	1.8	92.1	11.6	0.11

F1: <1 mm (0Ø); F2: <1/16 mm (+4Ø); sØ: sorting; aØ: skewness (Walker 1984); MdØ: median diameter (50% Ø)

the area of the volcano's flanks, they should have wavelengths in the 100- to 200-m range. Extrapolation of this kind probably has little physical reality, however, because gravity waves cannot reach such high wavelengths at the velocities which are realistic for the volcano's flanks. However, on the flanks of the volcano very long wavelength bed forms are evident within the limited exposures.

The decrease in wavelength and amplitude of surge dunes is a measure of the decreasing kinetic energy or carrying capacity of surge clouds with distance from the crater (Schmincke et al. 1973). In the case of the small Ubehebe and Taal surges, the wavelength decreases at a rate of 40—100 cm/km; for Peridot Mesa and Crater Elegante the rate is about 700 cm/km (Wohletz and Sheridan 1979). In comparison, the wavelength of the El Chichon surges decreases by about 2300 cm/km over the studied range, presumably reflecting a much higher initial velocity of the surge clouds.

Grain size characteristics

The grain size distribution of nine samples of the surge deposits was studied by wet-sieving of the coarse fraction and a particle data analyzer for the <20 μm fraction. All the samples are vertical channel samples through the deposit and thus represent the bulk grain-size distribution. At two localities the upper and lower half of the S-2 surge were sampled separately (EC-69 and 70, EC-62 and 63, Table 2). Results of the grain-size analysis are presented in Table 1 and in grain-size and component histograms in Figs. 14—16.

With respect to sorting and median grain size, the El Chichon surges S-1 and S-2 are not significantly different and fall in the midrange of other studied dune-bedded surge deposits (Walker 1984). They are poorly sorted, with sØ of 1.32—2.93, but skewness is weak or absent throughout the median grain size range (Fig. 17). The relatively low content of fine ash (<1/16 mm) in the El Chichon surges is comparable to that of the Mount St. Helens blast deposit and other surges in general (Walker 1984), but much lower than in typical pyroclastic flow deposits. The loss of fine glassy ash by winnowing is consistent with the results of modal analyses of the surges presented in the next section. Such fines elutriation should, however, lead to a skewed grain-size population, but the surges show no significant skew. We infer, therefore, that the original grain-size population in the surge-generating eruption cloud was nega-

Table 2. Modal fractions in weight %

Sample no.	km	Glass	Felsic xtls	Mafic xtls	Lithics
Surge S-1:					
EC-207	5.9	26.6	30.5	19.5	23.5
EC-193	7.5	22.3	29.6	15.1	33.1
EC-206	8.2	21.2	30.8	18.0	30.1
Surge S-2:					
EC-160	3.5	21.0	33.8	21.6	23.5
EC-69 (upper)	4.8	22.8	34.3	22.6	20.4
EC-70 (lower)	4.8	23.0	33.7	19.7	23.6
EC-102	5.0	19.6	24.4	15.4	40.6
EC-62 (upper)	6.3	21.2	34.3	21.0	23.5
EC-63 (lower)	6.3	15.2	36.7	24.5	22.6
Crushed pumice:					
EC-178		85.8	8.3	6.0	
Crushed lithics:					
EC-CL			14.2	7.6	78.4

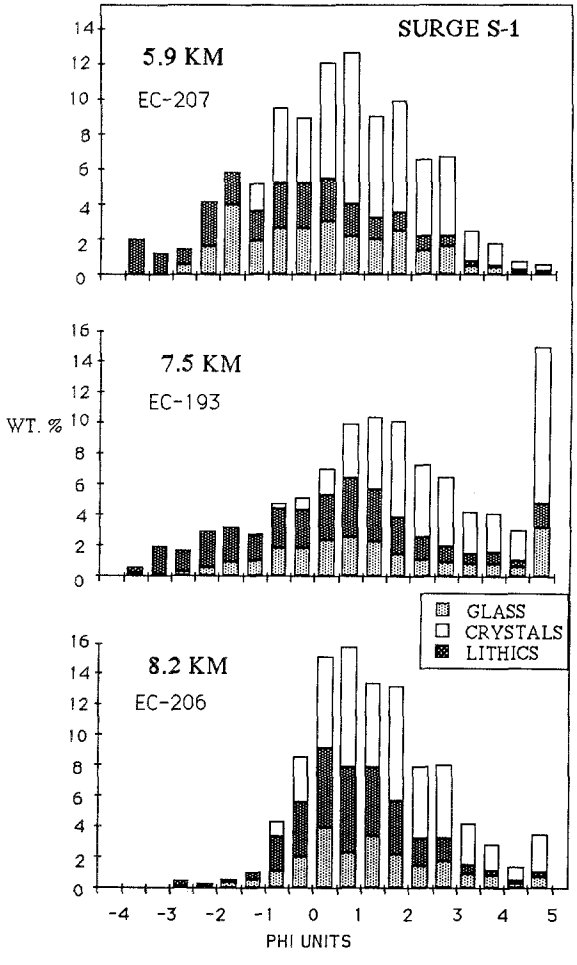

Fig. 14. Grain-size distribution and modal composition of the S-1 surge deposit in bulk samples from 5.9 km (EC-207), 7.5 km (EC-193), and 8.2 km (EC-206) from the crater. Modal components are crystals *(clear)*, lithics *(dark)*, and glass *(gray)*

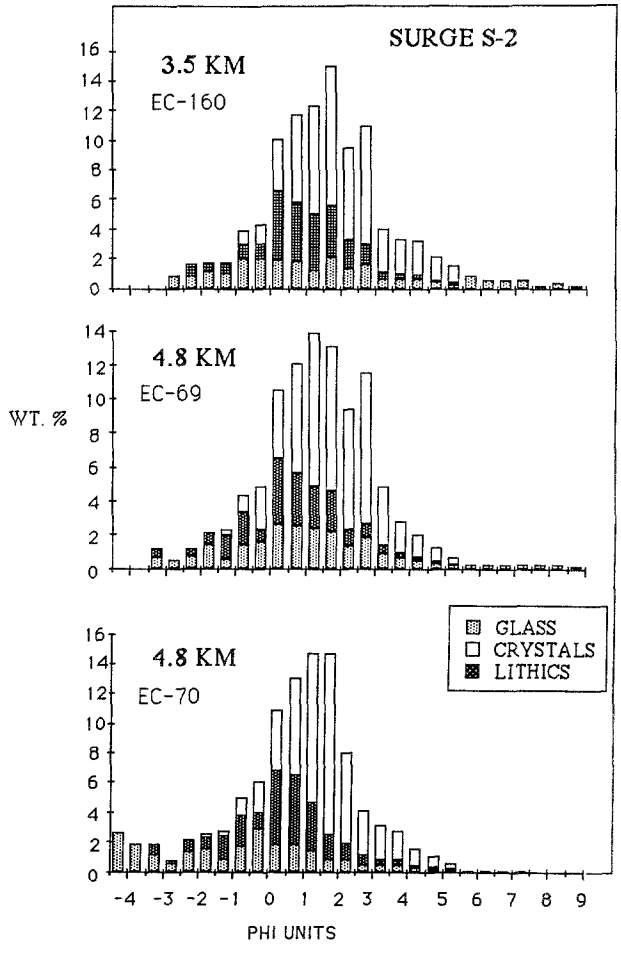

Fig. 15. Grain-size distribution and modal composition of the S-2 surge deposit in bulk samples collected 3.5 km from the crater (EC-160) and of bulk samples of the upper half (EC-69) and lower half (EC-70) of the S-2 surge layer at 4.8 km distance. Symbols for modal components as in Fig. 14

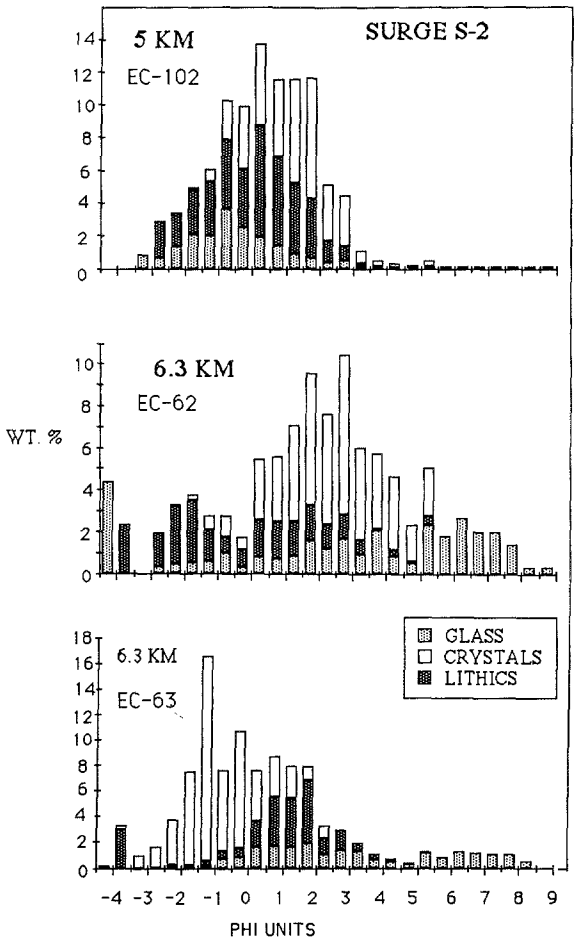

Fig. 16. Grain-size distribution and modal composition of bulk samples from the S-2 surge deposit at 5 km distance from source (EC-102) and of samples of the upper (EC-62) and lower (EC-63) part of the surge at 6.3 km distance. Symbols for modal components as in Fig. 14

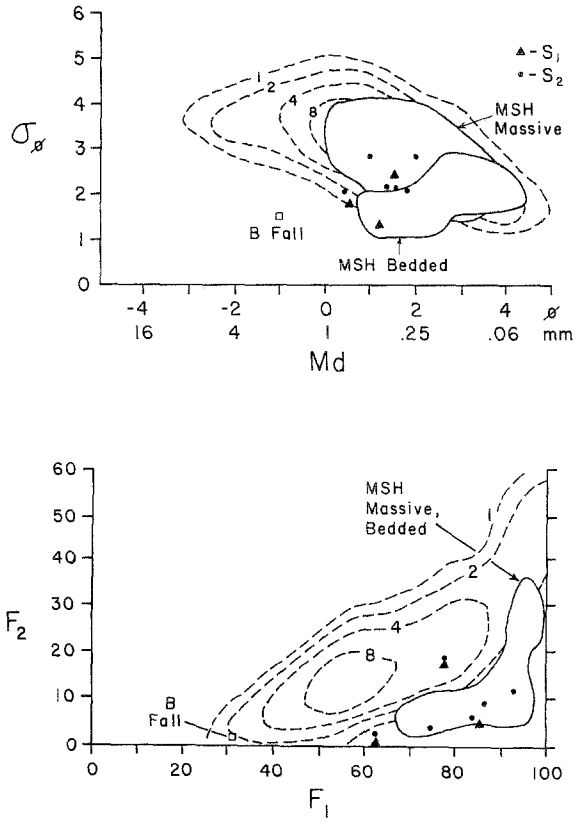

Fig. 17. Plot of grain-size data for the S-1 and S-2 El Chichon surge deposits. *Top,* graphic standard deviation (sØ) versus median diameter (MdØ). *Bottom,* F_2 (wt% less than 1 mm diameter) versus F_1 (wt% less than 1/16 mm diameter). *Dashed* contours are fields of pyroclastic flows and solid-outlined fields define bedded and massive blast deposits from the May 18 1980 eruption of Mount St. Helens, from Walker and McBroom (1983). *Open square* is data for the El Chichon B tephra-fall layer

tively skewed, and thus similar to the total grain-size distribution in the Mount St. Helens 1980 eruption cloud (Carey and Sigurdsson 1982).

Variations of several grain-size parameters with distance from source based on nine samples of the S-1 and S-2 surges are shown in Figs. 18 and 19. No significant variations in median diameter (MdØ), sorting (sØ), and skewness (aØ) are observed over the sampled range 3.5—8.5 km from the crater. Similarly, there is no systematic variation in the content of fines with distance from source, with F1 (size fraction <0 Ø) and F2 (size fraction $<+4$ Ø) varying in a random manner within narrow limits.

In contrast to the lack of dependence on distance from the vent in the grain-size data collected from sieve analysis, the diameter of maximum lithic fragments systematically decreases with distance (Fig. 20). The 1-kg bulk samples collected for grain-size analyses were therefore too small to be representative of the coarse fraction of the deposits.

Variations in MdØ and sØ with distance from source were also studied in the base surges of Taal volcano by Waters and Fisher (1971). Unlike the El Chichon surges, samples from the relatively small Taal dune forms show a steady decrease in median diameter and improved sorting with distance over the 2-km range studied.

The average of the maximum diameter of the five largest lithics fragments within a 0.5-m^2 horizontal cross section of the deposit was measured in the field. The results show that there is an order of magnitude decrease in lithics diameter over the range studied. On the whole, lithics in S-2 are smaller than in S-1 and the average diameter de-

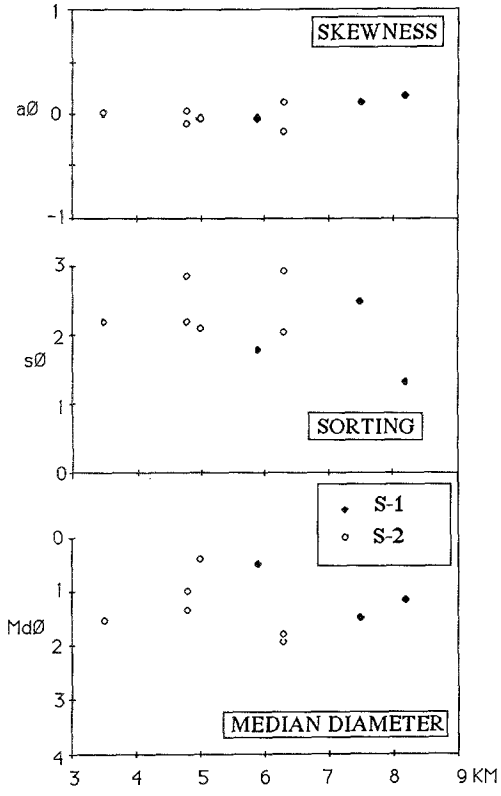

Fig. 18. Plots of sorting (sØ), skewness (aØ), and median diameter (MdØ) for El Chichon surges as a function of distance from source. *Filled* symbols are S-1 surge; *open* symbols are S-2 surge. The median diameter (MdØ) is the phi value at the 50 wt% level on the cumulative grain-size distribution curve

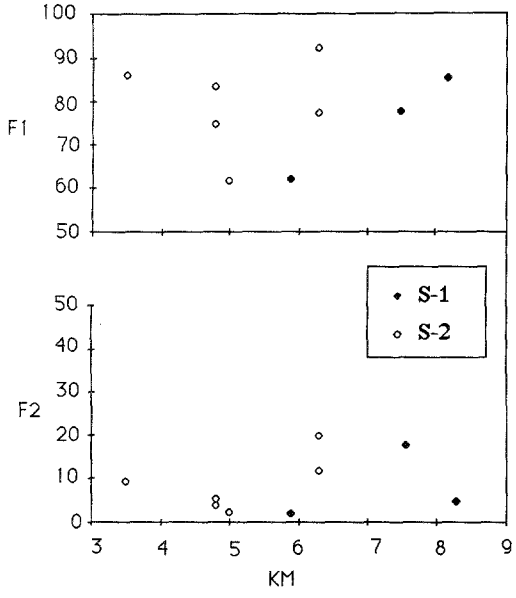

Fig. 19. Fines-depletion plots for El Chichon surges as a function of distance from source. F1 is the wt% finer than 1 mm (0 Ø) and F2 is wt% finer than 1/16 mm (+4 Ø)

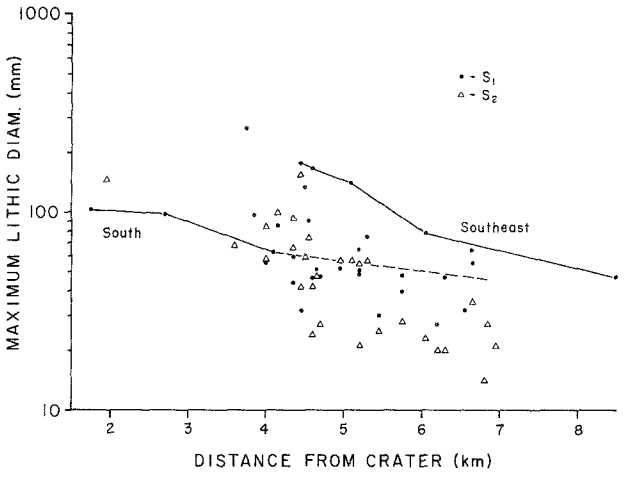

Fig. 20. Variation in maximum diameter of lithics (average of five largest clasts) as a function of distance from source in El Chichon surge deposits. Lithic variations along transects south and southeast of the volcano are also shown. The variation in lithic diameters in the Mount St. Helens blast deposit is after Hoblitt et al. (1981)

creases more rapidly, indicating a lower carrying capacity of this surge. The systematic decrease in lithic diameters in the S-1 surge was studied in two radial transects to the south and southeast of the volcano (Fig. 20). In these transects, the lithic diameter decreases at rates of 20—40 mm/km in the 2—8-km range, corresponding to about 25%/km decrease in mass of the largest transported lithics. In the S-2 surge, the rate of decrease in lithic diameter is higher, corresponding to about 33%/km decrease in the mass of the largest transported lithics. The second surge was thus both weaker and lost kinetic energy more rapidly than the first surge.

Modal components

The surge deposits consist of a mixture of glassy and vesicular pumice, free felsic and mafic crystals, and lithic fragments eroded from the volcano's conduit and vent or picked up from the near-vent surface. The relative abundance of these components in the surges contains useful information about selective fractionation of particles with different densities due to processes within the surge clouds. The modal fractions of crystals, pumice (mostly glass), and lithics have been determined by counting under a binocular stereoscope, for all grain-size fractions coarser than 5.5 Ø. The results are presented in histograms in Figs. 14—16 and summarized in Table 2. The val-

ues presented for *pumice* in the coarser fractions include glass plus any small crystals enclosed in the pumice fragment. Thus, these values tend to overestimate the glass content. Similarly, the proportion of lithics in the finer size fractions is underestimated because the contribution of free crystals derived from the fragmentation of porphyritic trachyandesite lithics is not taken into account.

The modal components are unevenly distributed among the various grain-size fractions, as is evident from the histograms in Figs. 14—16. Crystals and lithics dominate in the 0—3-Ø size range, whereas the pumice component typically has a wider size range. The bulk modal fractions of nine samples of the S-1 and S-2 surges (Table 2) show no significant differences, either between surges or as a function of distance from source. They are dominated by the felsic and mafic crystal components, which range 40—60 wt%, and 20—40 wt% lithics fragments. Pumice is thus the smallest component in the surges ranging 15—27 wt%. In order to compare the juvenile glass (pumice) and crystal content of the surges to that in the magma, we have subtracted the lithics and associated crystals. Mechanically crushed lithic blocks (sample EC-CL) have a modal lithic/crystal ratio of 3.6 and crystals have been subtracted from the bulk surge modal analyses in this proportion to derive an estimate of the juvenile crystal and glass components. These calculations indicate that the crystal/pumice ratio in the surges, after subtraction of the lithics, is in the range of 1.7—1.9. In contrast, the glass content in the juvenile magma has been estimated as ca. 47 wt% by least-squares mixing calculations based on whole-rock, glass, and mineral compositions giving a juvenile crystal/glass ratio of 1.1.

As stated above, modal analysis is likely to yield high apparent estimates of the pumice fraction owing to crystals enclosed in small pumice fragments. In order to evaluate this potential error, we mechanically crushed individual large pumices from the fall deposit (EC-178) and determined the modal proportions in the various grain-size fractions in the same manner as for the surges. This yielded an apparent glass fraction of 85 wt% in the crushed pumice or a crystal/pumice ratio of 0.17, indicating that the glass fraction is significantly overestimated in modal analysis due to the problem of crystals enclosed in glass.

While the bulk crystal/glass ratio thus cannot be accurately determined in the coarser fractions of the surge deposits because of cryptic crystals, the relative crystal enrichment factor of the surges can be established by comparison of modal analyses of the same size fractions in the crushed pumice and the surges. The procedure followed in arriving at the crystal enrichment factor for each grain-size fraction of the surges was, first, the proportion of crystals associated with the lithics was determined from the crystal/lithics ratio in each grain-size fraction for a mechanically crushed lithic block from the deposit (EC-CL). Typically, 10%—20% of the crystals are associated with the lithics. The proportion of crystals associated with the lithics in each size range was then subtracted from the total crystal content. The resulting corrected crystal/pumice ratio for the surge was then compared with the crystal/pumice ratio in the corresponding grain-size fraction of the mechanically crushed pumice to obtain a crystal enrichment factor.

The corrected enrichment factors for three samples of each surge are plotted in the grain-size spectrum in Fig. 21. It is clear that the surges show crystal enrichment relative to the crushed juvenile pumice by a factor of 2—4 for most of the grain-size classes with systematically higher enrichment factors for the S-2 surge deposit. Assuming that no crystals were lost from the surge cloud, the results indicate that a minimum of 40%—70% of the glass fraction was winnowed out prior to deposition of the surges. This corre-

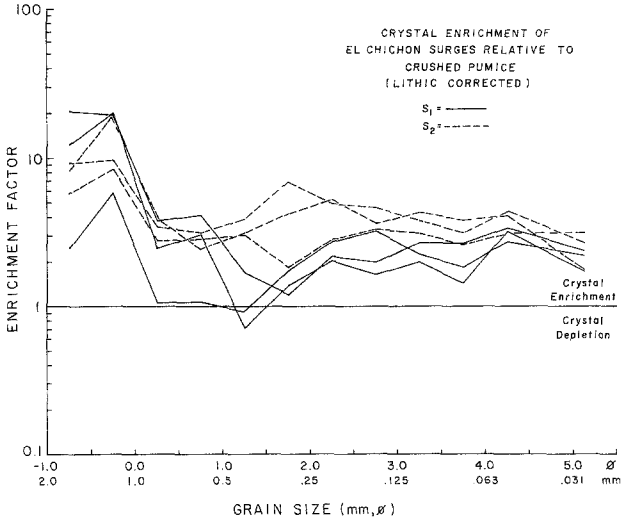

Fig. 21. Crystal enrichment in El Chichon surge deposits relative to crushed pumice. Data has been adjusted for crystals derived from crushed lithics. Note that crystal enrichment is characteristic of all the samples studied, indicating major elutriation of the glass fraction from the surge clouds. Also note higher enrichment factor in the 1—2-mm size range, which may be due to fractionation in the eruption column, as discussed in text

sponds to about 10%—25% decrease in the mass of the deposit. In the coarse grain-size range (>0 ∅) the enrichment factor is even larger, typically 10—20. These grain-size fractions represent, however, a small portion of the deposit.

The higher enrichment factor, i.e., greater pumice loss for the coarse fraction, is most probably related to the decreasing density of particles with increasing grain size. In the finer fractions, glass fragments are mostly nonvesicular and have densities closer to that of crystals and lithics. In the >0-∅ fractions the micropumices are sufficiently large to contain vesicles and have densities significantly lower than crystals of same size, leading to more efficient glass fractionation of this size range from the surge clouds.

The modal analyses therefore indicate that the original surge clouds consisted of about 35% lithics (including associated crystals), together with juvenile glass and crystals in roughly equal proportions. A minimum of 10%—25% of the surge cloud mass was lost prior to deposition of the surge, judging from crystal enrichment in the surge deposit relative to crushed juvenile pumice. It is likely that loss occurred in two ways, i.e., by fallout from the eruption column and by winnowing from the surge cloud. Loss of the coarse fraction (>0 ∅) is unlikely to have occurred in the surge cloud, and we propose that this fraction was selectively lost in the eruption column, whereas the finer fraction was lost by both mechanisms. Much of this fine material was transported as a dilute ash cloud beyond the surge zone, but owing to their small volume, the cosurge ash falls cannot be differentiated from the Plinian fall deposits.

The systematically higher crystal-enrichment factor for the S-2 surge indicates greater winnowing of glass fines from the second surge cloud, which may relate to the different mode of origin of the two surges. While S-1 formed from an explosion directly from the crater, S-2 immediately followed deposition of a Plinian fall layer and its origin has therefore been attributed to column collapse (Sigurdsson et al. 1984). It is possible that during evolution of the S-2 surge cloud, the eruption column was more expanded with higher incorporation of air and subsequently greater amount of winnowing from this surge.

Discussion

Surge clouds are high-velocity, highly expanded particulate fluids, which leave relatively thin deposits as compared with pyroclastic flow deposits. The bed forms within surge deposits reflect processes that take place primarily within the boundary layer at the base of the particulate fluid. The boundary layer is characterized by strong vertical velocity gradients caused by basal friction or drag forces and by strong gradients in particle concentration and grain size due to gravitative settling from the surge flow. In addition to transport by turbulent flow, which dominates in the surge cloud, particles into the boundary-layer bed load region may move by saltation and traction during the last stages of sedimentation. We believe that the latter processes are particularly important in the formation of El Chichon sand waves, as discussed in a later section.

A model for the El Chichon surges has to account for a number of observed features. Firstly, the deposits are dune bedded throughout most of their extent, with sand waves characterized by stoss-side erosion and lee-side deposition. Secondly, internal fabric of the sand waves is dominated by reversely graded, lee-side laminae, with extensive pumice rounding. Thirdly, despite the incorporation of large quantities of air, the surge clouds retained sufficient heat to carbonize wood throughout the area. Furthermore, lateral facies variations occur in the proximal area from true pyroclastic flows to surge deposits with a thick, somewhat massive, more poorly sorted central part, which in turn grade laterally into better sorted sand waves with distance from source. Finally, depletion of the pumice fraction in the >1.0 ∅ grain-size range has occurred, in addition to winnowing of the glass fraction in the finer grain-size range. Overall sorting of the surge deposits is intermediate between pyroclastic flows and pumice fall deposits. Based on these criteria, we propose a model for the El Chichon surges, which considers both the nature of particle transport and the processes of deposition.

Flow mechanisms

There is general agreement that pyroclastic surges are relatively low-concentration density currents, where particles are supported by turbulence (e.g., Sparks 1976; Fisher 1979; Walker and McBroome 1983). Sheridan and Updike (1975) and Wohletz and Sheridan (1979) have proposed that surges are initially lean-phase fluidized systems, which deflate due to escape of gases, resulting in transitions from viscous to inertial flow and rapid deposition. They concluded that the facies variations in bed forms, observed as a function of dis-

tance from source in some surge deposits, reflected this transition from viscous to inertial flow.

Following Wilson (1980, 1984), we define a truly fluidized system as consisting of a mixture of particles suspended by an upward escaping gas or fluid, where the drag force exerted by the gas is equal to the weight of the particles. In such a system the particle support is by fluidization. We note that this differs, e.g., from the definition of Sheridan and Updike (1975), who define the fluidized state as a mixture of particles suspended in a fluid phase such that the whole mass behaves as a fluid. In this definition the particle support is not necessarily by true fluidization, but may be due to internal turbulence in the system.

The behavior of pyroclastic particulate mixtures during fluidization has been studied by Wilson (1980, 1984), and his experimental results provide a basis for evaluating the hypothesis that El Chichon surge clouds may initially have been analogous to lean-phase fluidized systems. Experiments have shown that the fluidization behavior of pyroclastic mixtures is strongly dependent on gas flow and grain-size distribution. In very poorly sorted mixtures, the grain-size variation is so large that full fluidization is not attained but hysteresis occurs, leading to loss of the smallest particles by elutriation before the larger particles are fluidized. The grain sorting limit for full fluidization is near 1.5 s$\varnothing$. Moore poorly sorted materials cannot be fluidized but will tend to this value by means of fines elutriation during partial fluidization (Wilson 1984). In partly fluidized systems analogous to pyroclastic flows, the gas-flow velocity is sufficiently high to lead to some bed expansion, but not high enough to cause extensive elutriation. Voidage in such flows may be 0.1—0.4, with an upper limit of 0.7 depending on grain-size distribution (Wilson 1984). Sheridan and Updike (1975) suggested that the majority of base surge clouds are dilute phase fluidized systems with voidage >0.9. Wohletz and Sheridan (1979) also estimated the voidage in lean-phase fluidized beds, which they consider analogous to pyroclastic surges as >0.9. A similar solids concentration is calculated for the El Chichon surges, although as discussed below, this does not imply that the surges were fluidized systems. The trimline of the El Chichon surge zone indicates that the upper surface of the runout cone of the surges had a slope of 6° (Sigurdsson et al. 1984). This allows an estimate of the volume of the surge cloud (estimated density of 0.018 g/cm^3), which turns out to be 90 times the volume of the surge deposit (density of 1.6 g/cm^3). Thus, the voidage fraction in the surge deposit and the bulk surge cloud are 0.39 and 0.99, respectively.

The high gas-flow velocities required to induce such high voidage in a lean-phase fluidized system would be expected to result in extensive elutriation of the surge cloud, judging from the experimental results of Wilson. The evidence of the modal components in the El Chichon surge deposits shows that a minimum of 10%—25% of the particle fraction was lost during elutriation. However, if a fluidization process was operating in the El Chichon surges, we might expect, by analogy with Wilson's experiments, that fluidization and elutriation would have led to markedly improved sorting. This is not the case, however, as sorting in the surges averages 2.2 s$\varnothing$, which is very much higher than the 1.5 s$\varnothing$ grain sorting limit of fluidization proposed by Wilson (1980). This indicates that the surge cloud is better described as a highly expanded turbulent mixture in which the dominant particle support is by turbulence and saltation, a conclusion supported by theoretical considerations and analyses of the 18 May 1980 Mount St. Helens blast deposit (Fisher and Valentine 1986).

In summary, there are two factors which indicate that deposition from a lean-phase fluidized system sensu stricto may not be the appropriate model for the El Chichon surges and that a clear distinction between the overriding surge cloud and the bed load transported within meters of the ground may be required. Firstly, pumice rounding in the surges demonstrates the importance of attrition due to grain interactions, either during saltation or during inertial grain flow in a traction carpet. The degree of rounding due to transport in a dilute-phase, truly fluidized system such as an eruption column is negligible, as shown by pumices of the fall deposits. Rounding is therefore a feature characteristic of transport in the surge. Secondly, the very poor sorting of the surge deposits is not consistent with the elutriation and sorting behavior at high gas-flow rates in experimental studies on fluidized systems (Wilson 1980), as discussed above.

Saltation and transport in a traction-load layer are critical to the development of the sand-wave bed forms under surge clouds. The high degree of grain rounding in the El Chichon surge deposits indicates that rolling, sliding, and saltation of grains along the substrate were particularly important processes. There are important exceptions to this generalization, however, when the origin of the pyroclastic flows is considered. There is good

field evidence that small volume pyroclastic flows were associated with the emplacement of the surges. The stratigraphic relations are best reconciled by invoking a dense, basal, laminar-flow layer, which developed from the initial density current, whether derived directly from the crater (S-1) or from eruption column collapse (S-2, S-3). This basal component was channelled into gorges and valleys to form pyroclastic flows, whereas the great majority of the pyroclastic cloud remained internally dispersed by turbulence and spread over the flanks of the volcano as a low-concentration surge. There is also field evidence to suggest that the boundary separating these two different flow regimes was not sharp. A pyroclastic flow in the center of the S-2 surge in the proximal area can be traced laterally into a massive and poorly sorted surge unit, which merges into a stratified and cross-bedded, better sorted surge unit in the distal area. Thus, it appears that a continuum of particle concentration existed in the basal portion of the cloud. This continuum was, however, of limited extent, as indicated by the small volume of pyroclastic flows. The field evidence indicates that deposition from the dense, basal, laminar-flow layer of the density current was restricted to proximal areas.

Occurence of sand waves out to the distal margins indicates that the surge cloud persisted as a turbulent sediment gravity flow. In the El Chichon surge clouds, inertial forces were important at the base of the cloud in the proximal area, where particle concentration due to gravitational segregation was very high. As sedimentation occurred, the density of the overlying cloud was reduced. Another factor which tends to decrease the density of the overlying cloud is the entrainment of air. A pyroclastic gravity flow such as the El Chichon surge clouds can be viewed as a fluid which has a nonlinear density mixing relationship with an ambient fluid into which it is introduced (i.e., the atmosphere). As air is entrained into the surge cloud, it is heated by suspended pyroclasts and expands. If sedimentation is concurrently taking place, the resultant mixture can have a lower density than either of the two initial end members. Laboratory experiments on fluids with nonlinear density mixing relationships show that convective *clouds* are formed over density currents and that inflation and not deflation is a natural consequence of this process (Huppert et al. 1986). With simple thermal balance calculations, it is possible to evaluate the amount of air entrained and its volume change as a result of heat transfer from the hot, dispersed pyroclasts. The heat content of the surge at its initiation is the product of its mass, specific heat, and temperature at eruption (assumed to be 850° C). To cool to a temperature of 400° C (temperature required to carbonize vegetation at the distal end of the surge), the surge could mix with 2 times its *mass* of ambient air at 25° C (Fig. 22a). The volume change of the entrained air associated with heating to the lower temperature (400° C) would be approximately 18 times the original volume of the surge (Fig. 22b). These calculations indicate that in spite of the large amount of entrained air the

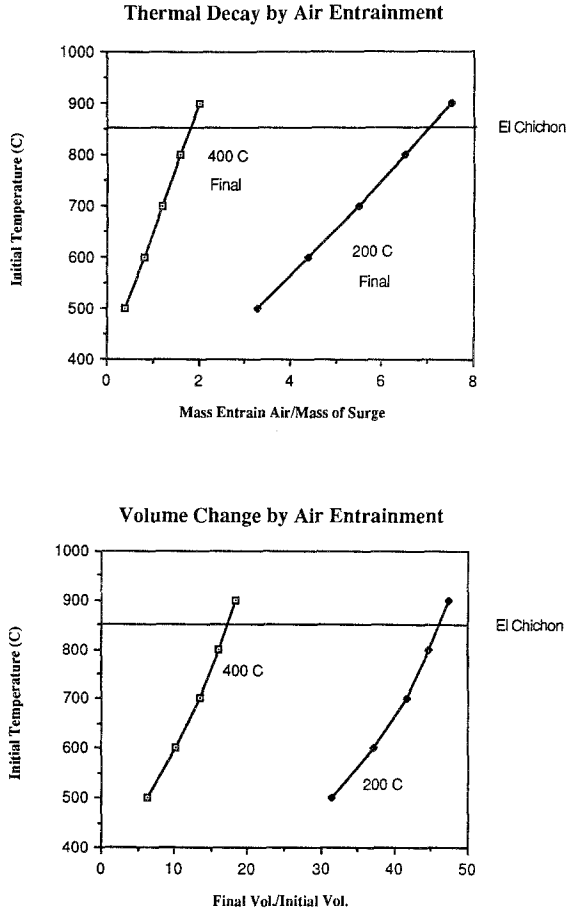

Fig. 22. a The effects of varying initial and final surge temperature on the ratio of mass entrained air/mass of surge. Initial temperature is the temperature of the pyroclastic and gas mixture issuing from the vent; final temperature is the temperature of the surge cloud at its distal end. The El Chichon 1982 surges with an estimated initial temperature is 850° C, could mix with 2 times their mass of air before cooling below 400° C, or about 7 times their mass of air before cooling below 200° C. **b** The change in volume of air entrained in the surge due to heat transfer from pyroclasts. At an initial temperature of 850° C the air in the El Chichon surges would increase in volume approximately 18 times before the surge clouds cooled below 400° C, and about 45 times at 200° C

surge cloud possessed sufficient heat content to maintain carbonizing temperatures throughout.

The balance between sedimentation at the base and expansion due to entrainment of air in the El Chichon surge clouds contributed to both low cloud density and internal turbulence to the distal edge of the surge zone. This contrasts with the deflation model of Wohletz and Sheridan (1979), which predicts a proximal to distal increase in the role of inertial versus viscous forces as the degree of fluidization is reduced.

Sedimentation processes

Some of the depositional processes occurring at the base of the El Chichon surge clouds can be inferred from the sedimentary features of the deposits and their lateral variation over the affected area. The large degree of particle rounding, presence of laminae, and formation of sand waves indicates that bed-load transport was important involving rolling, sliding, and saltation of grains in either turbulent or laminar flow. In addition, turbulent suspended-load transport must have been significant judging from the overall poor sorting of the deposits, winnowing out of fines, and the presence of massive units.

Surge deposits of some other volcanoes have been characterized as consisting of bed sets, separated by very fine ash-fall layers, most of which contain accretionary lapilli (Walker 1984). These relationships are not, however, observed in the El Chichon surge deposits, which are devoid of both accretionary lapilli and fine ash-fall beds. The El Chichon surge clouds were hot enough to carbonize wood throughout the area of deposition and too hot for condensation of vapor. Accretionary lapilli were therefore not formed and the fine ash elutriated from the density currents was deposited beyond the surge zone.

The El Chichon pyroclastic surges are characterized by wavy beds and dune forms throughout the area of deposition. In a few distal sections the laminae are indistinct owing to better sorting of the tephra, leading to a massive appearance of the thin surges in some outcrops. This pattern in the hot and dry El Chichon surges differs from the spatial succession of bed-form facies observed by Wohletz and Sheridan (1979) mainly in phreatomagmatic surge deposits.

The El Chichon surge deposits show evidence of variations in flow velocity of the surges with distance from source and velocity fluctuations with time. Firstly, both amplitude and wavelength of sand waves decrease with distance. This is accompanied by decrease in maximum diameter of lithics fragments, reflecting gradual deceleration of the surge. Secondly, in some sections of the deposits, the lower half of the surge layer is reversely graded and the upper half normally graded. This is accompanied in some outcrops by downrange dune-crest migration in the lower half, and uprange dune-crest migration in the upper half. We take this to indicate progressive increase in flow velocity leading to reverse grading and progressive downflow dune-crest migration, followed by decrease in flow rate in the second half of the surge, leading to overall normal grading and upstream dune-crest migration.

The sand waves deposited by the surge clouds of El Chichon are in some ways analogous to eolian bed forms such as ballistic ripples with pronounced stoss-side scour and lee-side deposition, and consequently, sedimentological models of transverse bed forms in eolian unidirectional flow can be considered in their mode of formation. There are, of course, important differences between the eolian and surge cloud processes of transportation, notably the higher mass flow and poorer sorting in the latter. Eolian fabrics are better sorted and indicate traction transport, whereas surge fabrics are more poorly sorted and indicate mass flow transport. In both instances, however, sand waves are formed. In the case of wet and consequently highly cohesive base surge clouds, the analogy with eolian processes is probably inappropriate (Schmincke et al. 1973). The El Chichon surge clouds were, on the other hand, hot and dry and the behavior of their bed load and suspended load was thus superficially analogous to wind-blown sand.

The El Chichon dunes externally resemble eolian dune forms such as ballistic ripples in overall aspect, but depositional fabrics differ from eolion fabrics. Ballistic ripples are bedforms which express a state of instability in the sediment flow, in contrast to the stable plane-bed configuration of sediment movement. Allen (1984) provides an excellent review of their character and origin. Small ballistic ripples have long, sinuoid form with horizontal form index (breadth/wavelength) up to 100. The horizontal form index declines with increasing grain size, stoss sides are more often weakly concave up, and the vertical profile tends to greater symmetry and crests become strongly curved and short. Ballistic ripples can reach wavelengths of 10—22 m in coarse-textured sediments (Hine and Boothroyd 1978) with wavelength increasing almost linearly with the

coarseness of the constituent sediment (Sharp 1963). To account for lee-side erosion, ballistic ripples are considered to have a recirculating quasi-steady lee eddy, generally several times longer than high, and a reattachment point somewhat higher up on the stoss than the base of the trough (Allen 1984). There is sediment transport downstream from a reattachment point to the next crest, where the grains are projected forward into the eddy.

The continuous transport of sediment over the crest of a sand wave creates a steady rain of particles on the leeward slope. As the deposition rate declines downstream, the effect of grain settlement is to progressively steepen the leeward slope. Steepening cannot proceed indefinitely, however, since there is a limiting slope, i.e., the angle of initial yield above which a surface underlain by the grains is unstable. A grain avalanche will consequently descend the slope, leaving the leeward surface inclined at a lower angle after shearing. This process should persist for so long as the rain of grains from above continues. Avalanching lowers the slope, whereas the downward rain steepens it, these tendencies opposing each other. However, as avalanches have a limited capacity to remove debris, traveling at a finite velocity, there should be a critical total load transport rate at the crest of the bed feature above which avalanching becomes continuous. Hence, the slip face may build forward either in discontinuous jerks, as one discrete avalanche after another descends, or in a continuous manner, as the result of the sustained and general downward flow of grains (Allen 1984). Avalanching can also lead to reverse grading in the lee-side laminae as larger grains migrate upward to the free surface when a mixture avalanches down a slope. Simultaneously, smaller grains tend to filter down between larger ones during flow, displacing larger grains upward by percolation, causing overall reverse grading of the individual laminae formed by each avalanche event (Bagnold 1954). This process has been proposed to account for inverse grading in pumice fall deposits which have slumped or avalanched down steep slopes (Duffield et al. 1979), but laminae formed this way should be well sorted. The morphology of El Chichon dune forms and presence of cm-scale, lee-side laminae suggests growth in a manner similar to the grain avalanching concept, but with modifications to take into account the more poorly sorted nature of the surge dunes.

Pyroclastic surges are considered to be relatively dilute, turbulent, sediment gravity flows (Fisher et al. 1986) where the sediment drives the system. During transport the surges develop a bed-load portion which increases concentration to such high level that the basal part of the system becomes weakly turbulent or nonturbulent. Because concentration is high, material within the bed load boundary zone is transported as thin grain flows, whereas within the surge above the bed load, coarse and fine material alike is being carried overhead in the more dilute suspension. The thin bed-load grain flows are analogous to the rapidly deposited bed load and avalanching layer described by Allen (1984) in the buildup of ballistic ripples. Whereas the avalanching layer of wind-blown sand develops within an environment where sorting will be excellent, high-concentration sediment gravity flows inhibit winnowing of grains, thereby resulting in poorly sorted deposits. Turbulence in wind-driven systems gives rise to traction and saltation movement and deposition. However, such sedimentary processes result from fluid gravity flows wherein the interstitial fluid carries the particles. In natural sediment gravity flows, the turbulent — or laminar — flow medium is composed of fluid-particle mixtures. Some particles may be too large to be carried within a turbulent eddy depending upon the density, viscosity, and velocity of the mixture, but can move by traction and saltation similar to particles in fluid gravity flows. The main bulk of particles, however, are an integral part of the fluid and may come to rest as small-scale grain flows in their last stages of motion. Traction and saltation transport are thus subdued with respect to particles small enough to be entrained within the fluid stream. We propose that this kind of modified eolian transport system meets the criteria of a sediment gravity flow and can produce thin, relatively poorly sorted, inversely graded, lee-side laminae.

Internal variations in particle concentration occurred in the surge cloud and are reflected in the deposition of coarse, poorly sorted lenses within stratified surge deposits which can be traced in the proximal direction to massive pyroclastic flows. Under conditions of high particle concentration, the bed-load transport over the crest of sand waves may exceed the finite transport rate by discrete avalanching, and continuous movement of sediment occurs down the lee side. Grain-dispersive forces within this bed-load material would also be expected to produce crude reverse grading, yet the large sediment load could retain poor sorting. This type of deposition was restricted to portions of the cloud which contained a high particle concentration and resulted

in massive lenses with texture of pyroclastic flows. They are most common where the surge cloud was channeled by preexisting topography, indicating that funneling of the surge cloud may have reduced the entrainment of air and in turn increased the particle concentration locally.

The vertical form index (ratio of wavelength to height) of El Chichon sand waves clusters mainly between 10 and 20 (Fig. 23). This is within the dominant range for sand waves from other pyroclastic surge deposits, such as Laacher See (Schmincke et al. 1973), Taal (Waters and Fisher 1971), and Ubehebe (Crowe and Fisher 1973) and unpublished data from ash-cloud surge deposits of the Bandelier Tuff (Fisher 1979). The vertical form index of volcanic sand waves has a relatively restricted range through a range in wavelength and amplitude of three orders of magnitude and involves sand waves produced by hot (dry) pyroclastic surges as well as base surges from pyroclastic eruptions which deposit cohesive (wet) materials. Moreover, there is a wide range in bedwave morphologies, many of which have such low-angle stoss- and lee-side slopes that avalanching could not occur. A similar vertical form index has been observed for ballistic ripples in general (e.g., Fig. 8-3 in Allen 1984), but some other eolian bed forms, such as Icelandic sand dunes, exhibit a much higher index (Hine and Boothroyd 1978).

Several factors have been proposed to account for variation in wavelength of eolian bed forms. According to the Velikanov-Mikhailova theory of ripple formation, the occurrence and equilibrium character of eolian dunes depend on the action and scale of the larger eddies of turbulence in a current (Yallin 1972). Larger eddies, having dimensions comparable with the boundary-layer thickness, are not only organized spatially along the flow, but are also correlated as to whether they scour or build up the bed. Yalin (1972) concluded that dune wavelength is approximately equal to $2\pi h$, where h is the boundary layer thickness. Thus, the boundary-layer thickness of El Chichon surges varies from ca. 5 m at 4 km to ca. 1 m at 6 km distance from source on the basis of this equation, and to up to 35 m near source (1.5 km) where wavelengths of 200 m can be extrapolated. The rapid decrease in erosion of tree stumps with height above ground 4—6 km from source supports a relatively small boundary-layer thickness. Other controls of wavelength which have been observed or proposed include wind shear, sediment coarseness, and length of saltation path (Ellwood et al. 1975). Wavelength increases with wind force and duration of wind action to a limit determined by sediment sorting. Wavelength also increases with sediment coarseness and with increasing textural disparity between the creeping and saltating loads. In the case of El Chichon sand waves, where grain-size variation is relatively minor, the deceleration of the surge cloud due to flow dissipation with distance from source is the most likely control of wavelength.

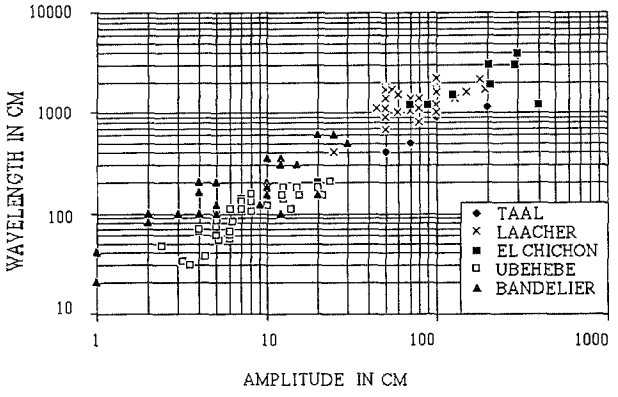

Fig. 23. Wavelength versus amplitude for El Chichon sand waves and other dune-bedded surge deposits. Taal data from Waters and Fisher (1971), Laacher See data from Schmincke et al (1973), and Ubehebe data from Crowe and Fisher (1973)

Conclusions

The gravity current origin of pyroclastic surges and pyroclastic flows is now well established, e.g., from their behavior during the 7 August 1980 Mount St. Helens eruption, when the flow-front velocity showed sensitive and direct response to topographic slope (Hoblitt 1986). The El Chichon flows and surges, whether derived directly from the crater (S-1 surge) or from eruption column collapse (S-2 and S-3 surges), were initially highly turbulent and sufficiently expanded to spread radially from the volcano's summit without regard for topography. Pyroclastic flow deposits represent only about 30% of the total combined mass of surges and flows from the 1982 eruptions (Sigurdsson et al. 1984). Thus, most of the pyroclastic debris remained internally dispersed by turbulence and spread over the flanks of the volcano as a low-concentration gravity-current surge with a minor portion of the current segregating into a dense basal laminar-flow layer, which was channeled into gorges and valleys and formed pyroclastic flows. Judging from the authors' observa-

tions of other well-known ignimbrite deposits (e.g., Crater Lake, Oregon; Bishop Tuff, California; Bandelier Tuff, New Mexico), the high proportion of pyroclastic surges over pyroclastic flows in the El Chichon eruptions is unusual, possibly related to a high volume rate of mixing of air into the current during rise and fall of the eruption column. As indicated by the large wavelength of El Chichon surges (Fig. 13), the gravity current must have been characterized by high radial velocity and great internal turbulence. The high velocity may be related to the height of eruption column collapse or high initial temperature of the current. On the other hand, base surge eruptions such as at Taal, Philippines, and at Laacher See, Germany, have produced deposits that have an even higher proportion of surge overflow deposits, but the reason for this is not clear.

The main body of the El Chichon density current advanced ahead of the channeled pyroclastic flows and formed a turbulent surge cloud, which spread quasi-radially up to 8 km from the crater as a dissipative flow. The principal causes of dissipation were reduction in slope, flow thickness, and density reduction due to sedimentation of pyroclasts, as evident from the progressive thinning of the surge deposit with distance from source (Figs. 7a and 7b).

Field evidence shows that the surge cloud remained sufficiently hot to carbonize wood in the distal area, where the deposit is only 2—3 cm thick, yet the evidence from the trim line indicates that a large quantity of air must have been incorporated and heated to account for the greatly expanded cloud. These observations may seem, at first, contradictory, but simple heat-budget calculations show that the heat content of the particle load is sufficient to heat the entrained air and maintain temperatures in the cloud high enough to carbonize wood. The heat content of the surge cloud is clearly the driving force of internal turbulence and incorporation of air, and it is likely that drag, associated with the expanding surge cloud as air is entrained and heated, is a factor which slows down the radial velocity and greatly influences dissipation of flow. As sedimentation reduces the bulk density and the entrained air expands as it is heated, the density contrast between the surge cloud and the surrounding atmosphere diminishes and the driving force for downslope movement disappears. There must be a point where the density is so low that the surge cloud ramps up, lifts off at the distal margin, and no longer travels along the ground.

The mode of transport of pyroclastic debris in the surge cloud can be inferred from the sedimentary structures and textural fabric of the deposit. The degree of large-particle rounding, presence of laminae, and formation of sand waves indicates that the bed-load transport mode was important involving mass flow of sand ribbons moving in essentially nonturbulent manner and moving larger particles with higher settling velocities in saltating and rolling motion similar to bed-load processes in streams or in sand storms. This high-concentration, sand-stream mode of movement at the boundary of the moving surge with the ground surface contributed to the poor sorting of the deposit as it built up at any particular locality. In addition, the suspended-load transport mode in turbulent flow must have been prominent judging from the overall poor sorting of the deposit, winnowing of fines, and the presence of massive units. During growth of sand waves, steady bed-load transport up the stoss side is probably turbulent and accompanied by stoss-side erosion. This continuous transport of pyroclastic grains creates a steady rain of particles over the crest or just leeward of the crest of the sand waves leading to progressive steepening of the leeward slope. When accumulation has resulted in a slope which exceeds the angle of initial yield, a pyroclastic avalanche descends the leeward slope and deposits a lamina, the basic building block of the sand wave. During avalanching, grain-dispersive pressures induced by shearing lead to reverse grading of each lamina (Bagnold 1954). In cases where flow separation leads to formation of a lee-side eddy or separation bubble, interaction between the backflow and the avalanche may affect the texture of the depositing lamina or cause lee-side erosion. El Chichon sand waves generally have quasi-parallel, lee-side laminae with few internal unconformities, indicating that erosion by the lee eddy is not important. The total bed-load transport rate over the crest may exceed the finite transport rate of discrete avalanches, in which case avalanching becomes continuous. Under conditions of such high flow rate, both bed-load and suspended-load transport lead to formation of a continuous pyroclastic flow layer, which advances over the sand waves and deposits relatively thick, very poorly sorted and coarser lee-side lenses analogous to thin pyroclastic flow units. Conditions for such high rates of concentrated flow are most favorable in the proximal area, where massive units in the central part of surge deposits grade laterally into true pyroclastic flows.

Acknowledgements. This work was supported by grants from the National Science Foundation (EAR-8416782) and the National Geographic Society. We thank Juan-Manuel Espindola, Winton Cornell, and David Gardella for assistance in the field. A thorough review of the manuscript by Armin Freundt is gratefully acknowledged.

References

Allen JRL (1984) Sedimentary Structures, Their Character and Physical Basis, Elsevier Amsterdam, 2 Vol

Bagnold RA (1954) The physics of blown sand and desert dunes. Methuen London 265 p

Brinkley SR Jr, Kirkwood JG, Lampson CW, Revelle R, and Smith SB (1950) Shock from underwater and underground blasts. In: The effects of Atomic Weapons. Ed S Glasstone. Los Alamos Scientific Laboratory Los Alamos NM US Gov Print Off 83—113

Carey SN, Sigurdsson H (1982) Influence of particle aggregation on deposition of distal tephra from the May 18 1980 eruption of Mount St. Helens volcano. J Geophys Res 87:7061—7072

Carey SN, Sigurdsson H (1985) The May 18 1980 eruption of Mount St. Helens 2. Modeling of dynamics of the plinian phase. J Geophys Res 90:2948—2958

Carey SN, Sigurdsson H (1986) The 1982 eruptions of El Chichon volcano, Mexico, 2: Observations and numerical modelling of tephra fall distribution. Bull Volcanol (in press)

Crow BM, Fisher RV (1973) Sedimentary structures in base-surge deposits with special reference to crossbedding, Ubehebe Craters, Death Valley, California. Geol Soc Am Bull 84:663—682

Duffield WA, Bacon CA, Roquemore GA (1979) Origin of reverse-graded bedding in air-fall pumice, Coso Range, California. J Volcanol Geotherm Res 5:35—48

Ellwood JM, Evans PD Wilson IG (1975) Small scale aeolian bedforms. J Sediment Petrol 45:554—561

Fisher RV (1979) Models for pyroclastic surges and pyroclastic flows. J Volcanol Geotherm Res 6:305—318

Fisher RV (1983) Flow transformations in sediment gravity flows. Geology 11:273—274

Fisher RV, Waters AC (1970) Base surge bedforms in maar volcanoes. Amer J Sci 268:157—180

Fisher RV, Heiken G (1982) Mt Pelee, Martinique: May 8 and 20, 1902 pyroclastic flows and surges. J Volcanol Geotherm Res 13:339—371

Fisher RV, Valentine J (1986) Pyroclastic flows surges and fluidization (abstr). Internat Volcanol Congress New Zealand, Feb 1—9, 1986

Fisher RV, Glicken HX, Hoblitt RP (1986) May 18, 1980 Mount St. Helens deposits in South Coldwater Creek, Washington. J Geophys Res (in press)

Hine AC, Boothroyd JC (1978) Morphology, processes, and recent sedimentary history of a glacial-outwash plain shoreline, southern Iceland. J Sed Petrol 48:901—920

Hoblitt RP (1986) Observations of the eruptions of July 22 and August 7, 1980, at Mount St. Helens, Washington. USGS Prof Pap (in press)

Hoblitt RP, Miller CD, Vallance JW (1981) Origin and stratigraphy of the deposit produced by the May 18 directed blast. In: Lipman PW, Mullineaux DR (eds) The 1980 eruptions of Mount St. Helens, Washington: US Geol Surv Prof Pap 1250:401—419

Hoblitt RP, Miller CD (1984) Comment. Geology 12:692—693

Moore JG (1967) Base surge in recent volcanic eruptions. Bull Volcanol 30:337—363

Moore JG, Sisson TW (1981) Deposits and effects of the May 18 pyroclastic surge. In: Lipman PW and Mullineaux DR (eds) The 1980 eruptions of Mount St. Helens, Washington: US Geol Surv Prof Pap 1250:421—438

Moore JG, Nakamura K, Alcaraz A (1966) The 1965 eruption of Taal volcano. Science 151:955—960

Richards AF (1959) Geology of the Islas Revillagigedo, Mexico 1. Birth and development of Volcan Barcena, Isla San Benedicto (1). Bull Volcanol 22:73—123

Schmincke H-U, Fisher RV, Waters AC (1973) Antidune and chute and pool structures in the base surge deposits of the Laacher See area, Germany. Sedimentology 20:553—574

Sharp RP (1963) Wind ripples. J Geol 71:617—636

Sheridan MF, Updike RG (1975) Sugarloaf Mountain tephra — a Pleistocene rhyolitic deposit of base-surge origin in northern Arizona. Geol Soc Am Bull 86:571—581

Sigurdsson H, Carey SN, Espindola JM (1984) The 1982 eruptions of El Chichon volcano, Mexico: stratigraphy of pyroclastic deposits. J Volcanol Geotherm Res 23:11—37

Sigurdsson H, Carey SN, Cornell W, Pescatore T (1985) The eruption of Vesuvius in AD 79. Nat Geogr Res 1:332—387

Sparks RSJ (1976) Grain size variations in ignimbrites and implications for the transport of pyroclastic flows. Sedimentology 23:147—188

Sparks RSJ, Walker GPL (1973) The ground surge deposit: a third type of pyroclastic rock. Nature 241:62—64

Sparks RSJ, Self S, Walker GPL (1973) Products of ignimbrite eruptions. Geology 1:115—118

Thorarinsson S, Einarsson T, Sigvaldason GSE, Elisson G (1964) The submarine eruption of the Vestmann Islands 1963—1964, a preliminary report. Bull Volcanol 27:1—11

Waitt RB Jr (1981) Devastating pyroclastic density flow and attendant air fall of May 18 — Stratigraphy and sedimentology of deposits. In: Lipman PW, Mullineaux DR (eds) The 1980 eruptions of Mount St. Helens, Washington. USGS Prof Pap 1250:439—458

Waitt RB Jr (1984) Comment, Geology 12:693

Walker GPL (1984) Characteristics of dune-bedded pyroclastic surge bedsets. J Volcanol Geotherm Res 20:281—296

Walker GPL, McBroome LA (1983) Mount St. Helens 1980 and Mount Pelee 1902 — flow or surge? Geology 11:571—574

Waters AC, Fisher RV (1971) Base surges and their deposits: Capelinhos and Taal volcanoes. J Geophys Res 76:5596—5614

Wilson CJN (1980) The role of fluidization in the emplacement of pyroclastic flows: an experimental approach. J Volcanol Geotherm Res 8:231—249

Wilson CJN (1984) The role of fluidization in the emplacement of pyroclastic flows, 2: Experimental results and their interpretation. J Volcanol Geotherm Res 20:55—84

Wohletz KH, Sheridan MF (1979) A model of pyroclastic surge. Geol Soc Am Spec Pap 180:177—194

Yalin MS (1972) Mechanics of sediment transport. Pergamon Oxford

Young GA (1965) The physics of the base surge. NOL TR 64-103, US Naval Ordnance Laboratory, White Oak, Md, p 284

Received February 25, 1986/Accepted October 27, 1986